

Biphasic character of ribosomal translocation and non-Michaelis-Menten kinetics of translation

Ping Xie*

*Key Laboratory of Soft Matter Physics and Beijing National Laboratory for Condensed Matter Physics,
Institute of Physics, Chinese Academy of Sciences, Beijing 100190, China*

(Received 28 June 2014; revised manuscript received 28 August 2014; published 1 December 2014)

We study theoretically the kinetics of mRNA translocation in the wild-type (WT) *Escherichia coli* ribosome, which is composed of a small 30S and large 50S subunit, and the ribosomes with mutations to some intersubunit bridges such as B1a, B4, B7a, and B8. The theoretical results reproduce well the available *in vitro* experimental data on the biphasic kinetics of the forward mRNA translocation catalyzed by elongation factor G (EF-G) hydrolyzing GTP, which can be best fit by the sum of two exponentials, and the monophasic kinetics of the spontaneous reverse mRNA translocation in the absence of the elongation factor, which can be best fit by a single-exponential function, in both the WT and mutant ribosomes. We show that both the mutation-induced increase in the maximal rate of the slow phase for the forward mRNA translocation and that in the rate of the spontaneous reverse mRNA translocation result from a reduction in the intrinsic energy barrier to resist the rotational movements between the two subunits, giving the same degree of increase in the two rates. The mutation-induced increase in the maximal rate of the fast phase for the forward mRNA translocation results mainly from the increase in the rate of the ribosomal unlocking, a conformational change in the ribosome that widens the mRNA channel for the mRNA translocation to take place, which could be partly due to the effect of the mutation on the intrasubunit 30S head rotation. Moreover, we study the translation rate of the WT and mutant ribosomes. It is shown that the translation rate versus the concentration of EF-G-GTP does not follow the Michaelis-Menten (MM) kinetics, which is in sharp contrast to the general property of other enzymes that the rate of the enzymatic reaction versus the concentration of a substrate follows the MM kinetics. The physical origin of this non-MM kinetics for the ribosome is revealed.

DOI: [10.1103/PhysRevE.90.062703](https://doi.org/10.1103/PhysRevE.90.062703)

PACS number(s): 87.15.A–

I. INTRODUCTION

In the cell, polypeptides are synthesized by the ribosome in a process called translation. Generally speaking, the elongation cycle of translation is composed of the following several steps. The ribosome selects an aminoacyl-transfer RNA (tRNA) molecule in the aminoacyl (A) site [1,2]. The aminoacyl-tRNA reacts with the peptidyl-tRNA in the peptidyl (P) site to form a peptide bond, resulting in deacylated tRNA in the P site and the peptidyl-tRNA prolonged by one amino acid in the A site. Catalyzed by elongation factor G (EF-G) hydrolyzing GTP, the A- and P-site tRNA molecules coupled with the messenger RNA (mRNA) via the codon-anticodon interaction are moved forward via coordinated translocation into the P and exit (E) sites, respectively [3–6]. Then the E-site deacylated tRNA is dissociated into the solution [7].

As the translocation of tRNA molecules coupled with the mRNA is one of the important steps in the translation elongation, the studies of the mechanism and kinetics of the translocation have attracted much attention. It was well characterized that the translocation takes place generally via two substeps, with the first one involving the transition of the ribosomal complex from the classical nonrotated to the rotated (or hybrid) pretranslocation state and the second one involving the transition from the hybrid to the post-translocation state [1–6]. Since both substeps of the translocation involve intersubunit rotations, i.e., the relative rotations between the small 30S and large 50S ribosomal subunits, studying the effect of the intersubunit rotations has strong implications for

understanding the molecular mechanism of the translocation. For example, using fluorescence-labeled mRNA, Liu and Fredrick [8] recently studied experimentally the effect of mutations to some intersubunit bridges such as B1a, B4, B7a, and B8 in the *Escherichia coli* ribosome, which are expected to constrain the intersubunit rotations, on the translocation kinetics. They found that as in the wild-type (WT) case [8–11], the EF-G-catalyzed forward mRNA translocation in the mutant ribosomes $\Delta B1a$, $\Delta B4$, $\Delta B7a$, and $\Delta B8$ also showed biphasic kinetics, which can be best fit by the sum of two exponentials, and the mutations increased both the maximal rates of the two phases and values of $K^{(1/2)}$, which is defined as the concentration of EF-G-GTP at which the half-maximal rate is obtained. Moreover, the mutations also increased the rate of spontaneous reverse mRNA translocation in the absence of the elongation factor. However, the detailed molecular mechanism underlying the correlation of the intersubunit rotations with the maximal rates of the two phases for the forward mRNA translocation and the rate of the spontaneous reverse mRNA translocation is not very clear. In addition, since besides the intersubunit rotations the forward mRNA translocation is also limited by a conformational change in the ribosome that widens the mRNA channel for the mRNA translocation to take place, which is termed ribosomal unlocking [12], it is interesting to determine how the mutations affect the ribosomal unlocking and moreover to distinguish the effect of the mutations on the intersubunit rotations and that on the ribosomal unlocking.

It is well known that the reaction rate of an enzyme versus the concentration of its substrate generally follows the Michaelis-Menten (MM) kinetics [13,14]. For example, it was well characterized that the movement velocity of the linear

*pxie@aphy.iphy.ac.cn

molecular motors such as kinesin and myosin versus ATP concentration, the replication rate of the DNA polymerase versus dNTP concentration, the transcription rate of the RNA polymerase versus NTP concentration, etc., follows the MM kinetics [14]. For the ribosome, with the single-molecule optical trapping, it was shown that in the small range of EF-G-GTP concentration (0–1 μ M) the experimental data on the rate of the ribosome translation of the mRNA with the homogeneous codons versus EF-G-GTP concentration can be approximately fitted by a MM equation [15]. However, a detailed theoretical analysis of this fit is still necessary. Moreover, it is unclear if in the large range of EF-G-GTP concentration the dependence of the translation rate on the EF-G-GTP concentration can still be fitted well by the MM equation. If the dependence does not obey the MM kinetics, then what is the physical origin for this non-MM dependence? This is an important issue because the dependence of the reaction rate of an enzyme on the concentration of its substrate has been an interesting topic since the landmark work of Michaelis and Menten (see, e.g., [16]).

The purpose of this paper is to address the above unclear issues. To the end, the paper is organized to be composed of two parts, with one focusing on the issues related to the mRNA translocation and the other focusing on the issues related to the translation rate in the elongation cycle. In the first part, based on the model of the mRNA translocation, which has been proposed before [17], we study theoretically the kinetics of the mRNA translocation in the WT and mutant ribosomes Δ B1a, Δ B4, Δ B7a, and Δ B8, reproducing the *in vitro* experimental data measured by Liu and Fredrick using fluorescence-labeled mRNA [8]. We show that both the mutation-induced increase

in the maximal rate of the slow phase for the forward mRNA translocation and that in the rate of the spontaneous reverse mRNA translocation result from the same degree of increase in the rates of the intersubunit rotations, which are in turn due to a reduction of the intrinsic energy barrier to resist the intersubunit rotations. Moreover, we show that the mutations also facilitate the ribosomal unlocking, resulting in the increase in the maximal rate of the fast phase for the forward mRNA translocation, and reduce the affinity of EF-G-GTP to the ribosome, resulting in the increase in values of $K^{(1/2)}$. In the second part, based on our results on the kinetics of the forward mRNA translocation, we study the translation rate of the WT and mutant ribosomes. Interestingly, we show that the translation rate versus the concentration of EF-G-GTP by the ribosome does not follow the MM kinetics, which is in sharp contrast to the general property by other enzymes that the rate of the enzymatic reaction versus the concentration of its substrate follows the MM kinetics. The non-MM kinetics of translation results from the intrinsic property of the spontaneous intersubunit rotations before EF-G-GTP binding to the pretranslocation ribosomal complex.

II. METHODS

A. Simplified model of EF-G-dependent forward mRNA translocation

In a previous work [17], we presented a simplified model to study the biphasic character of the forward mRNA translocation in the WT ribosome at a saturating concentration of EF-G-GTP. Here we use the model to study the kinetics of the mRNA translocation in WT and mutated ribosomes

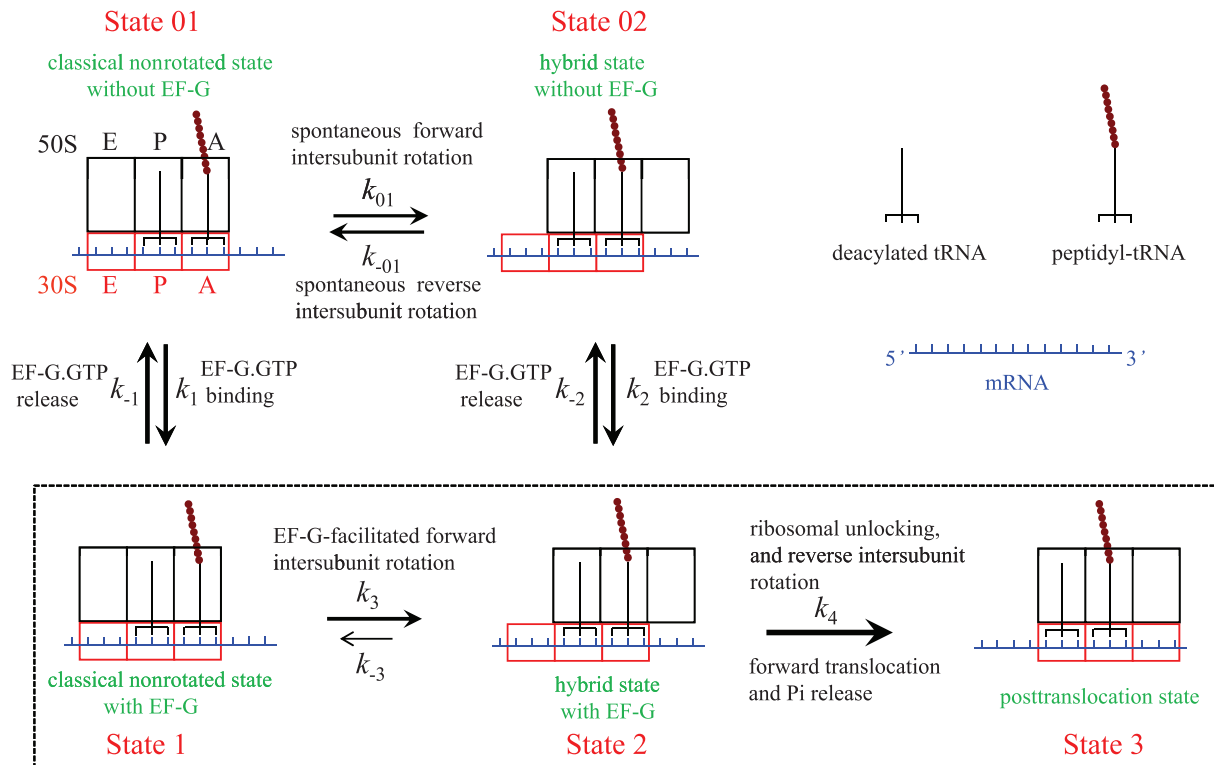


FIG. 1. (Color online) Simplified model of tRNA-mRNA translocation in the ribosome at nonsaturating concentration of EF-G-GTP (see the text for a detailed description). Represented inside the box are transitions at the saturating concentration of EF-G-GTP.

$\Delta B1a$, $\Delta B4$, $\Delta B7a$, and $\Delta B8$ at nonsaturating concentration of EF-G-GTP. For convenience, the model (Fig. 1) is redescribed as follows. Before EF-G-GTP binding, the ribosomal complex with deacylated tRNA bound to the 30S P site and the peptidyl-tRNA bound to the 30S A site can transit spontaneously between the classical nonrotated (state 01) and hybrid (state 02) states via the spontaneous forward and reverse intersubunit rotations, with the two states being in thermodynamic equilibrium with each other [18–23]. Here the forward intersubunit rotation refers to the rotation of the small 30S subunit in a counterclockwise direction (viewed from the exterior of the 30S subunit) relative to the large 50S subunit, while the reverse intersubunit rotation refers to the rotation of the small 30S subunit in the clockwise direction relative to the large 50S subunit. EF-G-GTP can bind to both states 01 and 02 [24,25]. (i) If EF-G-GTP binds to state 02, becoming state 2, after rapid GTP hydrolysis the ribosomal unlocking occurs, opening the mRNA channel in the 30S subunit. Then the reverse intersubunit rotation induces the movement of the two tRNA molecules coupled with the mRNA via the codon-anticodon interaction from the 30S A and P sites to the 30S P and E sites, respectively, while the two tRNA molecules are kept fixed to the 50S P and E sites by the high binding energy of the 50S E and P sites for the deacylated tRNA and peptidyl-tRNA, respectively [26–28]. This results in the transition to the post-translocation state (state 3). (ii) If EF-G-GTP binds to state 01, becoming state 1, the ribosomal complex then transits from state 1 to state 2 via the EF-G-facilitated forward intersubunit rotation, with a transition rate being mildly higher than that before EF-G-GTP binding [23]. Then, after the ribosomal unlocking, the reverse intersubunit rotation induces a transition from state 2 to state 3. As after the ribosomal unlocking the reverse intersubunit

rotation is very fast [12,29], the transition from state 2 to state 3 is rate limited by the ribosomal unlocking.

B. Pathway of translation elongation

With the translocation model shown in Fig. 1 and the other available biochemical data for tRNA binding and peptidyl transfer from the P-site peptidyl-tRNA to the A-site aminoacyl-tRNA, the minimal pathway for an elongation cycle of translation is shown in Fig. 2, where the transitions from state 01 through state 3 (inside the box) that are related to the EF-G-catalyzed mRNA-tRNA translocation are identical to those shown in Fig. 1. For simplicity of analysis, we consider only the translation of the mRNA with homogeneous codons using *in vitro* assays containing only one species of the ternary complex that is composed of the cognate aminoacyl-tRNA, elongation factor Tu (EF-Tu), and GTP. Thus, we neglect the competition of the cognate with the near-cognate and noncognate ternary complexes.

We begin the elongation cycle just after the peptidyl transfer. The ribosomal complex is now in the nonrotated pretranslocation state, with deacylated tRNA being in the P site of both subunits (P/P site) and the peptidyl-tRNA in the A/A site (state 01). The peptidyl transfer induces the ribosome to be labile [18–23], allowing the spontaneous intersubunit rotations before the binding of EF-G-GTP, with the ribosomal complex transiting from state 01 to state 02 and vice versa. EF-G-GTP can bind to both states 01 and 02, becoming states 1 and 2, respectively. State 1 then transits to state 2. In state 2 the ribosomal unlocking occurs, opening the mRNA channel. The subsequent reverse intersubunit rotation induces the transition of state 2 to state 3, with Pi release occurring independently. After transition to the post-translocation state 3, the mRNA

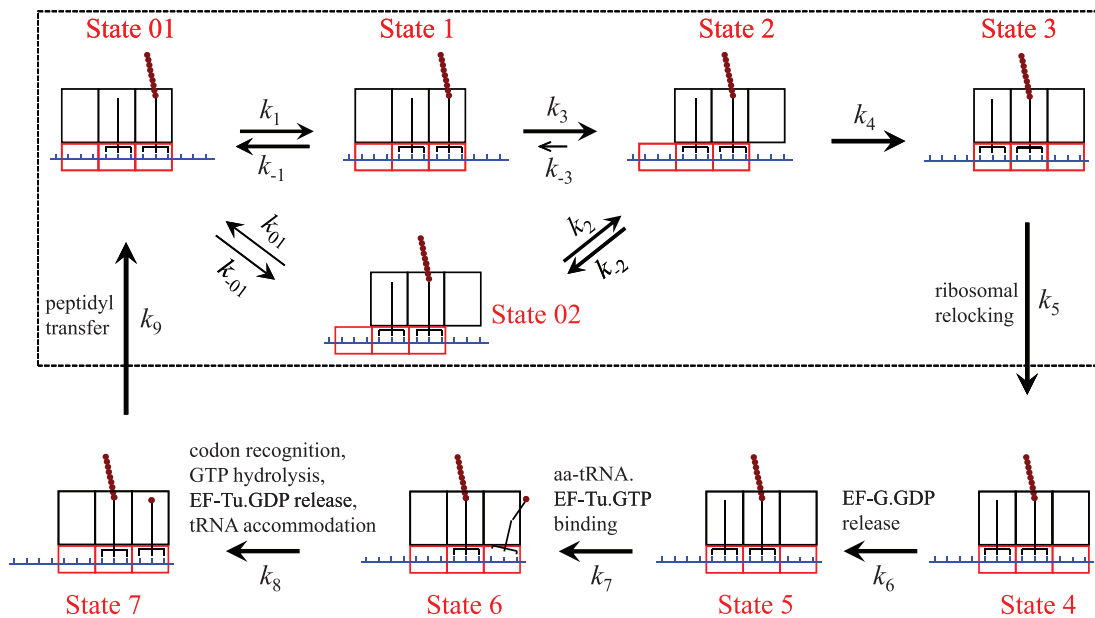


FIG. 2. (Color online) Minimal pathway of translation elongation at nonsaturating concentration of EF-G-GTP (see the text for a detailed description). We consider the translation of the mRNA with homogeneous codons using *in vitro* assays containing only the cognate ternary complex. We show here that the dissociation of deacylated tRNA occurs after the binding of the ternary complex, although the dissociation can occur at any state after the post-translocation [7].

channel in the 30S subunit becomes tight again, as proposed by Frank and Agrawal [30]. The occupation of the P/P site by the peptidyl-tRNA induces the ribosome to become locked or nonlabile [21] (state 4), constraining the intersubunit rotations. The locked ribosome facilitates EF-G-GDP release (state 5). The aminoacyl-tRNA-EF-Tu-GTP ternary complex then binds to the ribosome (state 6). After the codon recognition, GTP hydrolysis causes a large conformational change of EF-Tu, facilitating the accommodation of the aminoacyl-tRNA and the release of EF-Tu-GDP (state 7). Then the peptidyl transfer occurs, resulting in deacylated tRNA in the P/P site and the peptidyl-tRNA prolonged by one amino acid in the A/A site. Then the next elongation cycle proceeds.

C. Equations for kinetics of mRNA translocation

In this section we present equations for the kinetics of EF-G-catalyzed forward mRNA translocation under the condition as done in the *in vitro* biochemical assays with fluorescence-labeled mRNA molecules [8–11], where no ternary complex was present in the solution. In Fig. 1 we denote by P_{01} and P_{02} the probabilities of states 01 and 02 before the binding of EF-G-GTP, respectively, P_1 and P_2 the probabilities of states 1 and 2 after the binding of EF-G-GTP, respectively, and P_3 the probability of state 3. Then, from Fig. 1 the temporal evolutions of these probabilities are described by

$$\frac{dP_{01}(t)}{dt} = -(k_1 + k_{01})P_{01}(t) + k_{-01}P_{02}(t) + k_{-1}P_1(t), \quad (1)$$

$$\frac{dP_{02}(t)}{dt} = k_{01}P_{01}(t) - (k_{-01} + k_2)P_{02}(t) + k_{-2}P_2(t), \quad (2)$$

$$\frac{dP_1(t)}{dt} = k_1P_{01}(t) - (k_{-1} + k_3)P_1(t) + k_{-3}P_2(t), \quad (3)$$

$$\frac{dP_2(t)}{dt} = k_2P_{02}(t) + k_3P_1(t) - (k_{-2} + k_{-3} + k_4)P_2(t), \quad (4)$$

$$\frac{dP_3(t)}{dt} = k_4P_2(t), \quad (5)$$

where $k_1 = k_{b1}[\text{EF-G}]$, $k_2 = k_{b2}[\text{EF-G}]$, with k_{b1} and k_{b2} representing the binding rates of EF-G-GTP to states 01 and 02, respectively, and $[\text{EF-G}]$ representing the concentration of EF-G-GTP. It is noted that in the biochemical assays with fluorescence-labeled mRNAs to study the EF-G-catalyzed mRNA translocation [8–11], the experiments began with the addition of EF-G-GTP into the solution containing the pretranslocation ribosomal complex that is in either state 01 or 02, with the two states being in thermodynamic equilibrium, and stopped with the formation of the post-translocation state because of the absence of the ternary complex in the solution. In addition, since either before or after the release of EF-G-GDP from the post-translocation state the ribosome is kept unchanged relative to the mRNA, implying that the pyrene that is labeled at the 3' end of mRNA in the experiments [8–11] has the same fluorescence intensity. Thus, after the post-translocation, the ribosomal complex can be treated to be in the same state in the study of the ribosomal translocation under the condition of the experiments [8–11]. Consequently, to be consistent with these experimental conditions, there is

no transition coming from state 7 in Eq. (1) and none outgoing from state 3 in Eq. (5). Denoting by a the probability of the ribosomal complex in state 02 before adding EF-G-GTP into solution, the initial conditions at $t = 0$ are then as follows: $P_{01}(0) = 1 - a$, $P_{02}(0) = a$, and $P_1(0) = P_2(0) = P_3(0) = 0$, where time $t = 0$ represents the moment when the pretranslocation ribosomal complex is mixed with EF-G-GTP.

At saturating concentration of EF-G-GTP (inside the box in Fig. 1), the temporal evolutions of probabilities P_1 , P_2 , and P_3 have the forms

$$\frac{dP_1(t)}{dt} = -k_3P_1(t) + k_{-3}P_2(t), \quad (6)$$

$$\frac{dP_2(t)}{dt} = k_3P_1(t) - (k_{-3} + k_4)P_2(t), \quad (7)$$

$$\frac{dP_3(t)}{dt} = k_4P_2(t). \quad (8)$$

The initial conditions become $P_1(0) = 1 - a$, $P_2(0) = a$, and $P_3(0) = 0$. With these initial conditions, the analytical solution to Eqs. (6)–(8) have the forms [17]

$$P_3(t) = A_1[1 - \exp(-\lambda_1^{(\max)}t)] + A_2[1 - \exp(-\lambda_2^{(\max)}t)] \quad (9)$$

$$\lambda_1^{(\max)} = \frac{k_3 + k_{-3} + k_4}{2} + \frac{\sqrt{(k_3 + k_{-3} + k_4)^2 - 4k_3k_4}}{2}, \quad (10)$$

$$\lambda_2^{(\max)} = \frac{k_3 + k_{-3} + k_4}{2} - \frac{\sqrt{(k_3 + k_{-3} + k_4)^2 - 4k_3k_4}}{2}, \quad (11)$$

$$A_1 = \frac{(a - c)k_4}{\lambda_1^{(\max)}}, \quad (12)$$

$$A_2 = \frac{ck_4}{\lambda_2^{(\max)}}, \quad (13)$$

$$c = \frac{k_3(1 - a) + a(\lambda_1^{(\max)} - k_{-3} - k_4)}{\lambda_1^{(\max)} - \lambda_2^{(\max)}}. \quad (14)$$

It is noted that in order to compare with the *in vitro* experiments with the fluorescence-labeled mRNA, where only the change of $P_3(t)$ was monitored, for brevity we only give the solution of $P_3(t)$ here and the solutions of $P_1(t)$ and $P_2(t)$ are not given here.

D. Equations for translation rate in the elongation cycle

In the study of the translation rate in the elongation cycle, where both EF-G-GTP and the ternary complex are present in the solution, each transition in Fig. 2 must be taken into account. For convenience of the derivation of the translation rate based on Fig. 2, we consider separately the transition from state 01 to state 3 and the transition from state 3 to state 01. In addition, for simplicity, we only consider the ideal situation by neglecting the effect of the mRNA secondary structure that could be formed, the interaction of the nascent peptide with the exit tunnel, etc.

With the same procedure as that used in Ref. [7] or with the algebraic procedure, based on the elongation pathway (Fig. 2) we easily obtain that at steady state the mean time for the transition from state 3 to state 01 is calculated by

$$\tau_1 = \frac{1}{k_5} + \frac{1}{k_6} + \frac{1}{k_7} + \frac{1}{k_8} + \frac{1}{k_9}, \quad (15)$$

where $k_7 = k_b^{(\text{Tu})}[\text{aa-tRNA}]$, with $k_b^{(\text{Tu})}$ denoting the binding rate of the aminoacyl-tRNA–EF-Tu–GTP ternary complex and $[\text{aa-tRNA}]$ denoting the concentration of the ternary complex. Based on the elongation pathway (Fig. 2), with the algebraic procedure we obtain that at steady state the mean time τ_2 for the transition from state 01 to state 3 can be calculated by (see Appendix A)

$$\tau_2 = \frac{B + C[\text{EF-G}] + (k_3 + k_{-3} + k_4)k_{b1}k_{b2}[\text{EF-G}]^2}{k_4[k_{-01}k_3k_{b1} + k_{01}(k_{-1} + k_3)k_{b2}][\text{EF-G}] + k_3k_4k_{b1}k_{b2}[\text{EF-G}]^2}, \quad (16)$$

$$B = (k_{01} + k_{-01})(k_{-1}k_{-2} + k_{-1}k_{-3} + k_{-1}k_4 + k_{-2}k_3 + k_3k_4), \quad (17)$$

$$C = [k_{-01}(k_{-2} + k_3 + k_{-3} + k_4) + k_{-2}k_3]k_{b1} + [k_{01}(k_{-1} + k_3 + k_{-3}) + (k_{-1}k_{-3} + k_{-1}k_4 + k_3k_4)]k_{b2}. \quad (18)$$

With Eqs. (15)–(18) the translation rate $v = 1/(\tau_1 + \tau_2)$ is written as

$$v = \left(\frac{k_4[k_{-01}k_3k_{b1} + k_{01}(k_{-1} + k_3)k_{b2}]}{(k_3 + k_{-3} + k_4 + \tau_1k_3k_4)k_{b1}k_{b2}} + \frac{k_3k_4}{k_3 + k_{-3} + k_4 + \tau_1k_3k_4}[\text{EF-G}] \right) \times \left(\frac{B/[\text{EF-G}] + C + \tau_1k_4[k_{-01}k_3k_{b1} + k_{01}(k_{-1} + k_3)k_{b2}]}{(k_3 + k_{-3} + k_4 + \tau_1k_3k_4)k_{b1}k_{b2}} + [\text{EF-G}] \right)^{-1}. \quad (19)$$

From Eq. (19) it is evident that the dependence of the translation rate on the concentration of EF-G–GTP does not follow the MM kinetics. It is noted that if $k_{01} = k_{-01} = 0$, Eq. (19) is reduced to

$$v = \frac{k_3k_4}{k_3 + k_{-3} + k_4 + \tau_1k_3k_4}[\text{EF-G}] \left(\frac{k_{-2}k_3k_{b1} + (k_{-1}k_{-3} + k_{-1}k_4 + k_3k_4)k_{b2}}{(k_3 + k_{-3} + k_4 + \tau_1k_3k_4)k_{b1}k_{b2}} + [\text{EF-G}] \right)^{-1}. \quad (20)$$

Now the dependence of the translation rate on the concentration of EF-G–GTP follows the MM kinetics. Furthermore, if $k_{-2} = 0$, Eq. (20) is reduced to

$$v = \frac{k_3k_4}{k_3 + k_{-3} + k_4 + \tau_1k_3k_4}[\text{EF-G}] \left(\frac{k_{-1}k_{-3} + k_{-1}k_4 + k_3k_4}{(k_3 + k_{-3} + k_4 + \tau_1k_3k_4)k_{b1}} + [\text{EF-G}] \right)^{-1}. \quad (21)$$

This becomes the same as that derived in the literature [31,32]. Comparing Eq. (19) with Eq. (20), we thus note that the intrinsic property of the spontaneous intersubunit rotations before EF-G–GTP binding dictates the non-MM kinetics of the ribosome translation.

Equation (19) can be rewritten in another form

$$v = \frac{1}{\tau_0 + \tau_2}[\text{aa-tRNA}] \left([\text{aa-tRNA}] + \frac{1}{(\tau_0 + \tau_2)k_b^{(\text{Tu})}} \right)^{-1}, \quad (22)$$

$$\tau_0 = \frac{1}{k_5} + \frac{1}{k_6} + \frac{1}{k_8} + \frac{1}{k_9}. \quad (23)$$

From Eqs. (22) and (23) it can be clearly seen that at a given $[\text{EF-G}]$, the dependence of the translation rate on the concentration of the ternary complex follows the MM kinetics, with the MM constant $K_M^{(\text{Tu})} = 1/[(\tau_0 + \tau_2)k_b^{(\text{Tu})}]$ [33].

III. RESULTS

A. Biphasic kinetics of EF-G-dependent forward mRNA translocation

In this section we study the kinetics of EF-G-catalyzed forward mRNA translocation, comparing our theoretical results with the *in vitro* experimental data [8]. Before presenting our results, we first discuss the choice of values of some parameters. It is noted that values of EF-G–GTP binding rates k_{b1} and k_{b2} and EF-G–GTP release rates k_{-1} and k_{-2} should satisfy the relation $k_{b1}/k_{b2} = k_{-2}/k_{-1}$. Considering the available biochemical data of the EF-G–GTP binding rate of about $150 \mu\text{M}^{-1} \text{s}^{-1}$ and the EF-G–GTP-release rate of

about 140s^{-1} [1,12], here we take values of the four parameters satisfying $k_{b1}k_{-1} = k_{b2}k_{-2} \approx 20\,000 \mu\text{M}^{-1} \text{s}^{-2}$. Available single-molecule fluorescence resonance energy transfer (SMFRET) data showed that the binding of EF-G–GTP shifts the equilibrium toward the hybrid state, with k_3 increasing by about 2.3-fold and k_{-3} decreasing by about 10-fold [23]. Moreover, before the binding of EF-G–GTP, the majority of pretranslocation ribosomal complexes are in the hybrid state [23], implying $k_{01} > k_{-01}$. Thus, we take k_{-3} to be much smaller than k_3 . For simplicity, we fixed $k_{-3} = 0.04 \text{s}^{-1}$ for all ribosomes such as the WT, ΔB1a , ΔB4 , ΔB7a , and ΔB8 (noting that variations of k_{-3} have little effect on the

translocation kinetics provided $k_{-3} \ll k_3$). To be consistent with the SMFRET data [23], we take $k_{01} = k_3/2.3$. Before addition of EF-G–GTP into solution containing the pretranslocation ribosomal complex, the two states of the ribosomal complex, states 01 and 02 (Fig. 1), are in thermodynamic equilibrium. Thus, the two probabilities $P_{01}(0) = 1 - a$ and $P_{02}(0) = a$ and the transition rates k_{01} and k_{-01} should satisfy the equilibrium condition $k_{01}P_{01}(0) = k_{-01}P_{02}(0)$, i.e., $k_{01}/k_{-01} = a/(1 - a)$, from which the value of k_{-01} can be obtained. Thus, of the nine rate constants defined in Fig. 1 only four rate constants k_{b1}, k_{b2}, k_3 , and k_4 are adjustable.

First, we consider the WT ribosome. At a saturating concentration of EF-G–GTP, by adjusting $k_3 = 2.41 \text{ s}^{-1}$ and $k_4 = 14.96 \text{ s}^{-1}$ (see Table I), from Eqs. (10) and (11) we obtain $\lambda_1^{(\max)} = 15 \text{ s}^{-1}$ and $\lambda_2^{(\max)} = 2.4 \text{ s}^{-1}$, which are identical to the *in vitro* experimental data of Liu and Fredrick by using fluorescence-labeled mRNA [8]. Then, by adjusting $a = 0.582$, from Eqs. (12)–(14) we obtain $A_1 = A_2 = 0.5$, which is also consistent with the experimental data [8] showing that the fast phase accounts for 50%–70% of the total amplitude. The value of $a = 0.582$ implies that before the binding of EF-G–GTP the probability of the classical nonrotated state is $1 - a = 0.418$, which is consistent with the experimental data of about 0.41 ± 0.01 or 0.42 ± 0.01 obtained by Wang *et al.* [34].

At a nonsaturating concentration of EF-G–GTP, we take $k_{b1} = k_{b2} = 200 \text{ } \mu\text{M}^{-1} \text{ s}^{-1}$, from which values of k_{-1} and k_{-2} are determined (see Table I). From $k_3 = 2.41 \text{ s}^{-1}$ and $a = 0.582$, values of k_{01} and k_{-01} are determined (see Table I). We solve Eqs. (1)–(5) numerically using the Runge-Kutta method. Some results of $1 - P_3(t)$ versus time at different concentrations of EF-G–GTP are shown in Figs. 3(a)–3(c) (dots). It can be seen that the results at any [EF-G] can be well fitted by using a two-exponential function $1 - P_3(t) = A_1 e^{-\lambda_1 t} + A_2 e^{-\lambda_2 t}$, with fixed $A_1 = A_2 = 0.5$ independent of [EF-G]. The results of λ_1 and λ_2 versus [EF-G] are shown in Fig. 3(d), which can be fit to the MM equation

$$\lambda_i = \frac{\lambda_i^{(\max)} [\text{EF-G}]}{[\text{EF-G}] + K_i^{(1/2)}} \quad (i = 1, 2), \quad (24)$$

where $\lambda_1^{(\max)} = 15 \text{ s}^{-1}$, $\lambda_2^{(\max)} = 2.4 \text{ s}^{-1}$, $K_1^{(1/2)} = 0.73 \text{ } \mu\text{M}$, and $K_2^{(1/2)} = 0.22 \text{ } \mu\text{M}$. These data are in good agreement with the experimental data (see Table 3 in Ref. [8]).

TABLE I. Values of rate constants of ribosomal translocation for WT and mutant *Escherichia coli* ribosomes.

Rate constant	WT ^a	WT ^b	ΔB1a^b	ΔB4^b	ΔB7a^b	ΔB8^b
$k_3 (\text{s}^{-1})$	5.82	2.41	5.41	4.31	6.51	5.21
$k_{-3} (\text{s}^{-1})$	0.04	0.04	0.04	0.04	0.04	0.04
$k_4 (\text{s}^{-1})$	18.95	14.96	67.96	54.96	34.96	48.96
$k_{b1} (\mu\text{M}^{-1} \text{s}^{-1})$	80	200	130	140	55	60
$k_{b2} (\mu\text{M}^{-1} \text{s}^{-1})$	240	200	100	120	75	38
$k_{-1} (\text{s}^{-1})$	240	100	153.8	142.9	363.6	333.3
$k_{-2} (\text{s}^{-1})$	80	100	200	166.7	266.7	526.3
$k_{01} (\text{s}^{-1})$	2.53	1.05	2.35	1.87	2.83	2.27
$k_{-01} (\text{s}^{-1})$	1.34	0.75	0.87	1.01	1.52	1.51

^aValues under the experimental conditions of Walker *et al.* [36].

^bValues under the experimental conditions of Liu and Fredrick [8].

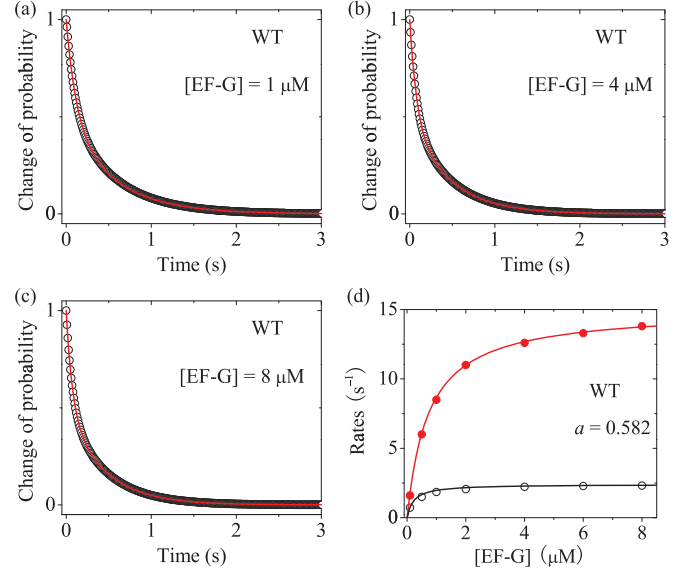


FIG. 3. (Color online) Results for the WT ribosome, with the probability of the hybrid state before EF-G–GTP binding being $a = 0.582$. (a)–(c) Change of the probability of the post-translocation state $1 - P_3(t)$ versus time at different concentrations of EF-G–GTP. Dots represent numerical results and red lines represent the fit curves with the two-exponential function $1 - P_3(t) = 0.5e^{-\lambda_1 t} + 0.5e^{-\lambda_2 t}$. (d) Rate of the fast phase λ_1 and rate of the slow phase λ_2 versus concentration of EF-G–GTP. Lines are fits to the MM equation $\lambda_{1,2} = \lambda_{1,2}^{(\max)} [\text{EF-G}] / ([\text{EF-G}] + K_{1,2}^{(1/2)})$, with $\lambda_1^{(\max)} = 15 \text{ s}^{-1}$, $\lambda_2^{(\max)} = 2.4 \text{ s}^{-1}$, $K_1^{(1/2)} = 0.73 \text{ } \mu\text{M}$, and $K_2^{(1/2)} = 0.22 \text{ } \mu\text{M}$.

As Eqs. (10)–(14) show, the variation of the hybrid-state probability a has no effect on the values of $\lambda_1^{(\max)}$ and $\lambda_2^{(\max)}$. Although the values of amplitudes A_1 and A_2 are dependent of the value of a [see Eqs. (9)–(14)], the numerical results show that for a fixed value of a , the values of A_1 and A_2 are approximately independent of [EF-G] (see Fig. 3). The MM constant for the rate of the fast phase versus [EF-G] only decreases slightly with the increase of a , while the MM constant for the rate of the slow phase versus [EF-G] is approximately independent of a (see Appendix B).

Second, we consider ΔB1a . At saturating [EF-G], by adjusting $k_3 = 5.41 \text{ s}^{-1}$ and $k_4 = 67.96 \text{ s}^{-1}$ (see Table I), from Eqs. (10) and (11) we obtain $\lambda_1^{(\max)} = 68 \text{ s}^{-1}$ and $\lambda_2^{(\max)} = 5.4 \text{ s}^{-1}$, which are identical to the experimental data of Liu and Fredrick [8]. The experimental data of Wang *et al.* [34] showed that for ΔB1a , the probability of nonrotated pretranslocation state before the binding of EF-G–GTP is about 0.27 ± 0.03 . Thus, we take $a = 0.73$, with which from Eqs. (12)–(14) we obtain $A_1 = 0.7$ and $A_2 = 0.3$, which are consistent with the experimental data of Liu and Fredrick [8] showing that the fast phase accounts for 50%–70% of the total amplitude. At nonsaturating [EF-G], we take $k_{b1} = 130 \text{ } \mu\text{M}^{-1} \text{ s}^{-1}$ and $k_{b2} = 100 \text{ } \mu\text{M}^{-1} \text{ s}^{-1}$ (see Table I), with which and $a = 0.73$ the other parameters are determined (see Table I). The numerical results of $1 - P_3(t)$ versus time at any [EF-G] can be well fitted by using the two-exponential function $1 - P_3(t) = A_1 e^{-\lambda_1 t} + A_2 e^{-\lambda_2 t}$ with fixed $A_1 = 0.7$ and $A_2 = 0.3$ (Fig. 4, the first row from the top). The results

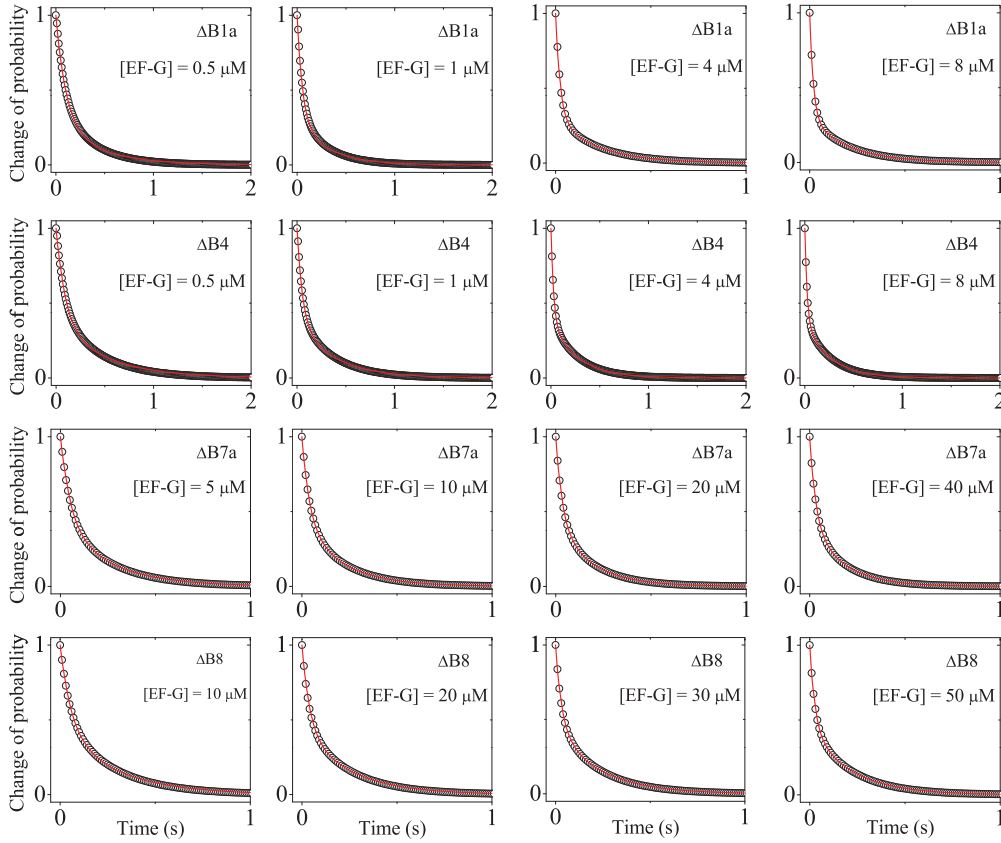


FIG. 4. (Color online) Results for the change of the probability of the post-translocation state $1 - P_3(t)$ versus time at different concentrations of EF-G–GTP for $\Delta B1a$ (the first row from the top), $\Delta B4$ (the second row), $\Delta B7a$ (the third row), and $\Delta B8$ (the fourth row). The probabilities of the hybrid state before EF-G–GTP binding are $a = 0.73$ for $\Delta B1a$, $a = 0.65$ for $\Delta B4$, $a = 0.65$ for $\Delta B7a$, and $a = 0.6$ for $\Delta B8$. Dots represent numerical results and red lines represent the fit curves with the two-exponential function $1 - P_3(t) = A_1 e^{-\lambda_1 t} + A_2 e^{-\lambda_2 t}$, where $A_1 = 0.7$ and $A_2 = 0.3$ for $\Delta B1a$, $A_1 = 0.62$ and $A_2 = 0.38$ for $\Delta B4$, $A_1 = 0.57$ and $A_2 = 0.43$ for $\Delta B7a$, $A_1 = 0.55$ and $A_2 = 0.45$ for $\Delta B8$, and λ_1 and λ_2 are shown in Fig. 5.

of λ_1 and λ_2 versus $[\text{EF-G}]$ are shown in Fig. 5(a), which can be fitted to Eq. (24), with $\lambda_1^{(\max)} = 68 \text{ s}^{-1}$, $\lambda_2^{(\max)} = 5.4 \text{ s}^{-1}$, $K_1^{(1/2)} = 2.4 \text{ } \mu\text{M}$, and $K_2^{(1/2)} = 0.67 \text{ } \mu\text{M}$. These are in good agreement with the experimental data (see Table 3 in Ref. [8]).

Similarly, for $\Delta B4$, by taking $k_{b1} = 140 \text{ } \mu\text{M}^{-1} \text{ s}^{-1}$, $k_{b2} = 120 \text{ } \mu\text{M}^{-1} \text{ s}^{-1}$, $k_3 = 4.31 \text{ s}^{-1}$, $k_4 = 54.96 \text{ s}^{-1}$, and $a = 0.65$ (see Table I), the numerical results of $1 - P_3(t)$ versus time at any $[\text{EF-G}]$ can be well fitted by using the two-exponential function, with fixed $A_1 = 0.62$ and $A_2 = 0.38$ (Fig. 4, the second row from the top). The results of λ_1 and λ_2 versus $[\text{EF-G}]$ are shown in Fig. 5(b), which can be fit to Eq. (24), with $\lambda_1^{(\max)} = 55 \text{ s}^{-1}$, $\lambda_2^{(\max)} = 4.3 \text{ s}^{-1}$, $K_1^{(1/2)} = 2.0 \text{ } \mu\text{M}$, and $K_2^{(1/2)} = 0.65 \text{ } \mu\text{M}$. These are in good agreement with the experimental data (see Table 3 in Ref. [8]). For $\Delta B7a$, by taking $k_{b1} = 55 \text{ } \mu\text{M}^{-1} \text{ s}^{-1}$, $k_{b2} = 75 \text{ } \mu\text{M}^{-1} \text{ s}^{-1}$, $k_3 = 6.51 \text{ s}^{-1}$, $k_4 = 34.96 \text{ s}^{-1}$, and $a = 0.65$, we obtain $A_1 = 0.57$, $A_2 = 0.43$, $\lambda_1^{(\max)} = 35 \text{ s}^{-1}$, $\lambda_2^{(\max)} = 6.5 \text{ s}^{-1}$, $K_1^{(1/2)} = 4.4 \text{ } \mu\text{M}$, and $K_2^{(1/2)} = 3.6 \text{ } \mu\text{M}$ [Figs. 4 and 5(c)], which are in good agreement with the experimental data (see Table 3 in Ref. [8]). For $\Delta B8$, by taking $k_{b1} = 60 \text{ } \mu\text{M}^{-1} \text{ s}^{-1}$, $k_{b2} = 38 \text{ } \mu\text{M}^{-1} \text{ s}^{-1}$, $k_3 = 5.21 \text{ s}^{-1}$, $k_4 = 48.96 \text{ s}^{-1}$, and $a = 0.6$, we obtain $A_1 = 0.55$, $A_2 = 0.45$, $\lambda_1^{(\max)} = 49 \text{ s}^{-1}$, $\lambda_2^{(\max)} = 5.2 \text{ s}^{-1}$, $K_1^{(1/2)} = 18 \text{ } \mu\text{M}$, and $K_2^{(1/2)} =$

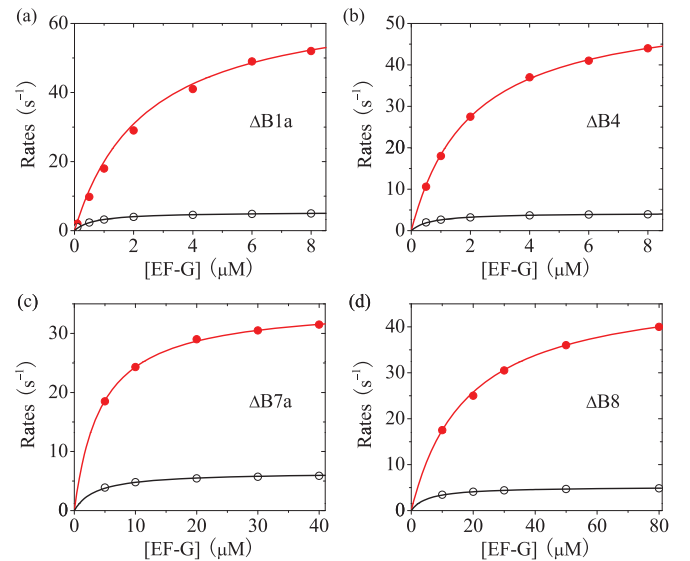


FIG. 5. (Color online) Results for the rate of the fast phase λ_1 of the forward mRNA translocation and the rate of the slow phase λ_2 versus concentration of EF-G–GTP for mutated ribosomes (a) $\Delta B1a$, (b) $\Delta B4$, (c) $\Delta B7a$, and (d) $\Delta B8$. Lines are fits to the MM equation $\lambda_{1,2} = \lambda_{1,2}^{(\max)} [\text{EF-G}] / ([\text{EF-G}] + K_{1,2}^{(1/2)})$.

5.4 μM [Figs. 4 and 5(d)], which are in good agreement with the experimental data (see Table 3 in Ref. [8]). In addition, by taking $k_{b1} = 260 \mu\text{M}^{-1} \text{s}^{-1}$, $k_{b2} = 260 \mu\text{M}^{-1} \text{s}^{-1}$, $k_3 = 1.51 \text{s}^{-1}$, $k_4 = 14.96 \text{s}^{-1}$, and $a = 0.552$, we obtain $A_1 = A_2 = 0.5$, $\lambda_1^{(\text{max})} = 16$, $\lambda_2^{(\text{max})} = 1.5 \text{s}^{-1}$, $K_1^{(1/2)} = 0.53 \mu\text{M}$, and $K_2^{(1/2)} = 0.15 \mu\text{M}$, which are in good agreement with the experimental data for reassociated 70S at 20 mM $[\text{Mg}^{2+}]$ (see Table 3 in Ref. [8]).

B. Correlation between the increase in the rate of the slow phase for the forward mRNA translocation and that of the spontaneous reverse mRNA translocation

In our model (Fig. 1), the rate of the slow phase for the forward mRNA translocation is approximately equal to the rate k_3 of the forward intersubunit rotation with the binding of EF-G-GTP [see Eq. (11) under $k_{-3} \ll k_3 < k_4$]. Consider that the mutation to the intersubunit bridge induces the two ribosomal subunits to rotate more easily with each other. This is equivalent to saying that the mutation reduces the intrinsic energy barrier to resist the intersubunit rotations. Denoting by ΔE the mutation-induced reduction in the intrinsic energy barrier, the forward transition rate k_3 for the mutated ribosomes ΔB1a , ΔB4 , ΔB7a , and ΔB8 can be approximately calculated by [29]

$$k_3 = C \exp\left(-\frac{E_{\text{NR}} - \Delta E}{k_B T}\right), \quad (25)$$

where C is a constant and E_{NR} represents the energy barrier for the nonrotated pretranslocation ribosomal complex bound with EF-G-GTP to change to the hybrid complex (i.e., the transition of state 1 to state 2) in the WT case.

As analyzed before [29], the spontaneous reverse mRNA translocation is equivalent to the thermal-noise-induced change of the nonrotated ribosomal complex in the nonlabile state to the rotated conformation in the absence of any elongation factor [35]. It is evident that this change gives a single-exponential decay in the probability of the post-translocation ribosomal complex, which is in contrast to the biphasic character of the EF-G-catalyzed forward mRNA translocation, as shown in Sec. III A. This monophasic kinetics of the spontaneous reverse translocation is also consistent with the experimental data [8]. Assuming that the mutations of the intersubunit bridges B1a, B4, B7a, and B8 have little effect on the locking strength of the post-translocation ribosomal complex, the energy barrier to resist the nonrotated ribosomal complex in the nonlabile state changing to the rotated conformation is also reduced by ΔE . Thus, the rate of the spontaneous reverse translocation k_b for the mutated ribosomes ΔB1a , ΔB4 , ΔB7a , and ΔB8 can be approximately calculated by [29]

$$k_b = C' \exp\left(-\frac{E_0 - \Delta E}{k_B T}\right), \quad (26)$$

where C' is a constant and E_0 represents the energy barrier for the WT ribosomal complex to change from the post-translocation to hybrid pretranslocation state in the absence of any elongation factor.

From Eqs. (25) and (26) it can be seen that the mutation increases the transition rate k_3 and the reverse translocation rate k_b by the same degree $\exp(\Delta E/k_B T)$ relative to those of

TABLE II. Values of rate constants of translation elongation for the *Escherichia coli* ribosome, which are taken from the available biochemical data [1,37–41].

Rate constant	Value
$k_5(\text{s}^{-1})$	5
$k_6(\text{s}^{-1})$	20
$k_b^{(Tu)} (\mu\text{M}^{-1} \text{s}^{-1})$	110
$k_8(\text{s}^{-1})$	2.7
$k_9(\text{s}^{-1})$	50

the WT case. This is consistent with the experimental data [8], as it is shown in the following. From our theoretical data given in Sec. III A, we see that the forward transition rates k_3 for ΔB1a , ΔB4 , ΔB7a , and ΔB8 are increased, respectively, by about 2.3-fold, 1.8-fold, 2.7-fold, and 2.2-fold relative to that for the WT case. By comparison, from Table II of Ref. [8], it is noted that the spontaneous reverse translocation rate k_b for ΔB1a , ΔB4 , ΔB7a , and ΔB8 is increased, respectively, by about 2.4-fold, 1.7-fold, 1.7-fold, and 2.0-fold relative to that for the WT case, which is consistent with the increase of k_3 . These increases in rate by about 2.3-fold, 1.8-fold, 2.7-fold, and 2.2-fold correspond to ΔE having values of about $0.83k_B T$, $0.59k_B T$, $0.99k_B T$, and $0.79k_B T$, respectively.

It is mentioned that in the above analysis we considered that the mutations of the intersubunit bridges B1a, B4, B7a, and B8 have little effect on the locking strength of the post-translocation ribosomal complex. If the mutations of the bridges such as B2a and B3 affect the locking strength of the post-translocation complex, Eq. (26) should be replaced by $k_b = C' \exp[-(E_0 - \Delta E + \Delta E_{\text{lock}})/k_B T]$, where ΔE_{lock} represents the mutation-induced increase in the energy to lock the ribosome in the nonrotated conformation. This provides an explanation of the experimental data showing that although for ΔB2a and ΔB3 the transition rate k_3 is increased, the spontaneous reverse translocation rate k_b is reduced [8]. From the experimental data of approximately 3.4-fold increase in k_3 (which is estimated from the data for the slow phase in Table 3 of Ref. [8]) and the approximately 1.55-fold decrease in k_b (which is estimated from the data in Table 2 of Ref. [8]) for ΔB2a and ΔB3 at 20 mM $[\text{Mg}^{2+}]$, we estimate $\Delta E = 1.22k_B T$ and $\Delta E_{\text{lock}} = 1.66k_B T$.

C. Non-Michaelis-Menten kinetics of translation

In this section we calculate the translation rate by using values of the parameters under the experimental conditions used by Liu and Fredrick [8], as determined in Sec. III A. We also use values of the parameters under the experimental conditions used by Walker *et al.* [36], which are determined as follows. As in Sec. III A, by taking $k_{b1} = 80 \mu\text{M}^{-1} \text{s}^{-1}$, $k_{b2} = 240 \mu\text{M}^{-1} \text{s}^{-1}$, $k_3 = 5.82 \text{s}^{-1}$, $k_4 = 18.95 \text{s}^{-1}$, and $a = 0.654$, from which values other related rate constants are determined (see Table I), we obtain $A_1 = 0.5$, $A_2 = 0.5$, $\lambda_1^{(\text{max})} = 19 \text{s}^{-1}$, $\lambda_2^{(\text{max})} = 5.8 \text{s}^{-1}$, $K_1^{(1/2)} = 0.36 \mu\text{M}$, and $K_2^{(1/2)} = 0.61 \mu\text{M}$, which are identical to the experimental data of Walker *et al.* [36]. For an approximation under the experimental conditions of Walker *et al.* [36] and of Liu and Fredrick [8], we take the same values of the parameters

k_5, \dots, k_9 , which are taken from the available biochemical data [1,37–41], as given in Table II.

First, we consider the WT case. With values of k_5, \dots, k_9 , as given in Table II, and values of other parameters under the conditions of Walker *et al.* [36], as given in Table I, using Eq. (19) we calculate the translation rate by the WT ribosome versus EF-G-GTP concentration at saturating ternary-complex concentration [aa-tRNA], with the results being shown in Fig. 6(a) (with $k_{01} \neq 0$ and $k_{-01} \neq 0$). For comparison, in Fig. 6(a) we also show the results calculated using Eq. (20) (with $k_{01} = k_{-01} = 0$). From Fig. 6(a) it can be seen that with $k_{01} \neq 0$ and $k_{-01} \neq 0$, the translation rate as a function of EF-G-GTP concentration deviates evidently from the MM kinetics, as noted from Eq. (19). However, with $k_{01} = k_{-01} = 0$, the translation rate as a function of EF-G-GTP concentration follows the MM kinetics, as can be seen from Eq. (20). Thus, the intrinsic property of the spontaneous transitions between the classical nonrotated and hybrid states before EF-G-GTP binding results in the non-MM kinetics of translation. Although the curve of translation rate versus [EF-G] in the wide range of [EF-G] deviates evidently from the MM form with $k_{01} \neq 0$ and $k_{-01} \neq 0$, the curve can be approximately fitted to the MM equation in the same small range of [EF-G] = 0–1 μM as that used in the experiment of Qu *et al.* [15], with the maximal translation

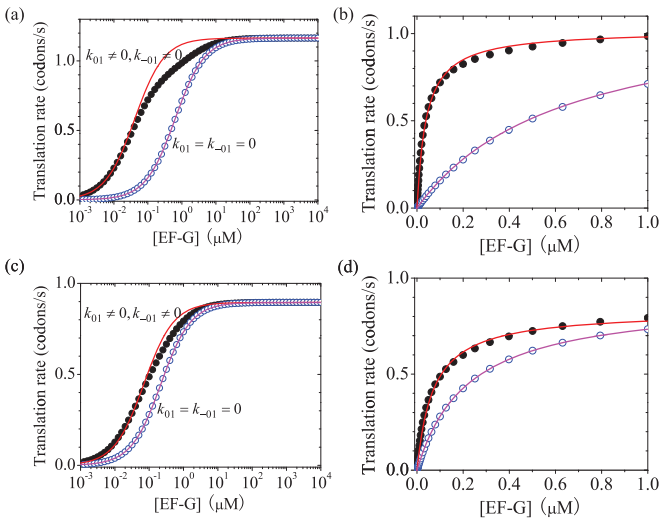


FIG. 6. (Color online) Translation rate by WT ribosomes versus EF-G-GTP concentration at saturating concentration of the ternary complex with (a) and (b) the parameter values under the conditions of Walker *et al.* [36], with (b) being the enlargement of (a), and (c) and (d) the parameter values under the conditions of Liu and Fredrick [8], with (d) being the enlargement of (c). Dots represent calculated results. Lines are fits to the MM equation $v = v^{(\max)}[\text{EF-G}]/([\text{EF-G}] + K_M^{(G)})$, where (a) $v^{(\max)} = 1.164 \text{ s}^{-1}$, and $K_M^{(G)} = 40 \text{ nM}$ with $k_{01} \neq 0$ and $k_{-01} \neq 0$, and $v^{(\max)} = 1.164 \text{ s}^{-1}$ and $K_M^{(G)} = 630 \text{ nM}$, with $k_{01} = k_{-01} = 0$; (b) $v^{(\max)} = 1.02 \text{ s}^{-1}$ and $K_M^{(G)} = 40 \text{ nM}$, with $k_{01} \neq 0$ and $k_{-01} \neq 0$, and $v^{(\max)} = 1.164 \text{ s}^{-1}$ and $K_M^{(G)} = 630 \text{ nM}$, with $k_{01} = k_{-01} = 0$; (c) $v^{(\max)} = 0.895 \text{ s}^{-1}$ and $K_M^{(G)} = 70 \text{ nM}$, with $k_{01} \neq 0$ and $k_{-01} \neq 0$, and $v^{(\max)} = 0.895 \text{ s}^{-1}$ and $K_M^{(G)} = 220 \text{ nM}$, with $k_{01} = k_{-01} = 0$; and (d) $v^{(\max)} = 0.83 \text{ s}^{-1}$ and $K_M^{(G)} = 70 \text{ nM}$, with $k_{01} \neq 0$ and $k_{-01} \neq 0$, and $v^{(\max)} = 0.895 \text{ s}^{-1}$ and $K_M^{(G)} = 220 \text{ nM}$, with $k_{01} = k_{-01} = 0$.

rate $v^{(\max)} = 1.02 \text{ s}^{-1}$ and the MM constant $K_M^{(G)} = 40 \text{ nM}$ [Fig. 6(b)]. These values are consistent with the available *in vitro* experimental data ($v^{(\max)} = 0.50 \pm 0.06 \text{ s}^{-1}$ and $K_M^{(G)} = 40 \pm 10 \text{ nM}$) on translation through the single-stranded mRNA with homogeneous codons measured by Qu *et al.* [15]. However, it is noted that the MM constant $K_M^{(G)} = 630 \text{ nM}$ with $k_{01} = k_{-01} = 0$ deviates significantly from the experimental data of $40 \pm 10 \text{ nM}$.

Similarly, under the conditions of Liu and Fredrick [8], the results of the translation rate by the WT ribosome versus EF-G-GTP concentration at saturating [aa-tRNA] are shown in Fig. 6(c) (in the wide range of [EF-G]) and Fig. 6(d) (in the small range of [EF-G] = 0–1 μM). It can be seen that the results under the conditions of Liu and Fredrick [8] [Figs. 6(c) and 6(d)] are similar to those under the conditions of Walker *et al.* [36] [Figs. 6(a) and 6(b)]. In the small range of [EF-G] = 0–1 μM , the curve of translation rate versus [EF-G] with $k_{01} \neq 0$ and $k_{-01} \neq 0$ can be approximately fitted to the MM equation, with the maximal translation rate $v^{(\max)} = 0.83 \text{ s}^{-1}$ and the MM constant $K_M^{(G)} = 70 \text{ nM}$ [Fig. 6(d)], which are close to the available experimental data ($v^{(\max)} = 0.50 \pm 0.06 \text{ s}^{-1}$ and $K_M^{(G)} = 40 \pm 10 \text{ nM}$) [15]. However, the MM constant $K_M^{(G)} = 220 \text{ nM}$ with $k_{01} = k_{-01} = 0$ deviates significantly from the experimental data of $40 \pm 10 \text{ nM}$. In the wide range of [EF-G], the curve deviates evidently from the MM form. In other words, even with $k_{b1} = k_{b2}$, the translation rate as a function of [EF-G] still does not follow the MM kinetics. This is because the rate of transition from the hybrid state (state 2) to post-translocation state (state 3) is different from the rate of transition from the classical nonrotated pretranslocation state (state 1) to post-translocation state (state 3). However, under the conditions of Liu and Fredrick [8], the curve of translation rate versus [EF-G] in the wide range of [EF-G] with $k_{01} \neq 0$ and $k_{-01} \neq 0$ is closer to the MM form than under the conditions of Walker *et al.* [36].

As shown above, in the real case with $k_{01} \neq 0$ and $k_{-01} \neq 0$ the dependence of the translation rate on [EF-G] does not obey the MM kinetics. By comparison, with $k_{01} = k_{-01} = 0$ the dependence obeys the MM kinetics. By comparing the two cases (Fig. 6) it can be seen that although at very high saturating [EF-G] the two cases give the same translation rate, at low [EF-G] (e.g., at [EF-G] = 0–1 μM), the translation rate with the non-MM kinetics is higher than that with the MM kinetics, providing a possible explanation of why the ribosome adopts the non-MM kinetics rather than the MM kinetics.

Equation (22) shows that at a given [EF-G], the translation rate versus the ternary-complex concentration [aa-tRNA] follows the MM kinetics. With values of k_5, \dots, k_9 , as given in Table II, and values of other parameters under the condition of Walker *et al.* [36], as given in Table I, using Eq. (22) the calculated MM constant of translation rate versus [aa-tRNA] at saturating [EF-G] is $K_M^{(\text{Tu})} = 10.5 \text{ nM}$, which is close to the experimental data of $5 \pm 2 \text{ nM}$ on translation through the single-stranded mRNA with homogeneous codons by Qu *et al.* [15]. Similarly, under the conditions of Liu and Fredrick [8], the calculated MM constant of translation rate versus [aa-tRNA] at saturating [EF-G] is $K_M^{(\text{Tu})} = 8.1 \text{ nM}$, which is also close to the available experimental data of $5 \pm 2 \text{ nM}$ [15].

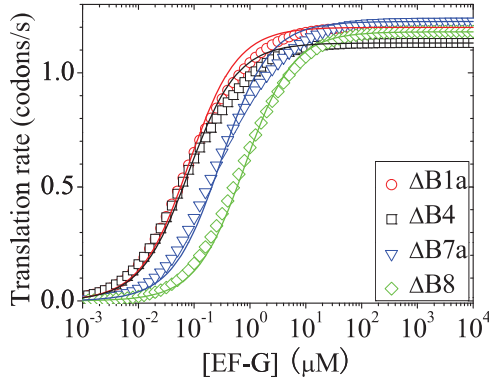


FIG. 7. (Color online) Translation rate by mutant ribosomes $\Delta B1a$, $\Delta B4$, $\Delta B7a$, and $\Delta B8$ versus EF-G-GTP concentration at saturating concentration of the ternary complex. Dots represent calculated results. Lines are fits to the MM equation $v = v^{(\max)}[\text{EF-G}]/([\text{EF-G}] + K_M^{(G)})$, where $v^{(\max)} = 1.2 \text{ s}^{-1}$ and $K_M^{(G)} = 80 \text{ nM}$ for $\Delta B1a$, $v^{(\max)} = 1.131 \text{ s}^{-1}$ and $K_M^{(G)} = 80 \text{ nM}$ for $\Delta B4$, $v^{(\max)} = 1.225 \text{ s}^{-1}$ and $K_M^{(G)} = 300 \text{ nM}$ for $\Delta B7a$, and $v^{(\max)} = 1.18 \text{ s}^{-1}$ and $K_M^{(G)} = 800 \text{ nM}$ for $\Delta B8$.

Then we consider the mutant ribosomes $\Delta B1a$, $\Delta B4$, $\Delta B7a$, and $\Delta B8$. With values of k_5, \dots, k_9 , as given in Table II, and values of other parameters under the condition of Liu and Fredrick [8], as given in Table I, using Eq. (19) we calculate the translation rate by the mutant ribosomes versus EF-G-GTP concentration at saturating [aa-tRNA]. The results are shown in Fig. 7. First, it can be seen that as for the WT case, the curves of the translation rate versus [EF-G] for the mutant cases do not have the MM forms. Second, by comparing Fig. 6 with Fig. 7 it can be seen that at saturating EF-G-GTP the mutant cases have larger translation rates than the WT case. Third, it can be seen that at saturating EF-G-GTP the translation rate by $\Delta B7a$ is slightly larger than that by $\Delta B1a$. By contrast, from the experimental data [8] it can be seen that at saturating EF-G-GTP, the rate of the fast phase for the forward mRNA translocation for $\Delta B1a$ is about 2-fold larger than that for $\Delta B7a$. Since in our model (Fig. 1) the translocation rate at saturating EF-G-GTP during the elongation cycle is mainly determined by the slow transition rate k_3 and is less sensitive to the fast transition rate k_4 , our results showing that the translation rate by $\Delta B7a$ is slightly larger than that by $\Delta B1a$ are consistent with the experimental data showing that the transition rate k_3 for $\Delta B7a$ is slightly larger than that for $\Delta B1a$.

If we fit the results of the translation rate versus EF-G-GTP concentration in Fig. 7 by using the MM equation, we obtain that the MM constant for $\Delta B1a$ ($K_M^{(G)} = 80 \text{ nM}$) is only slightly larger than that for the WT case ($K_M^{(G)} = 70 \text{ nM}$). By contrast, from the experimental data it can be seen that the MM constant for the rate of the fast phase for the forward mRNA translocation versus [EF-G] for $\Delta B1a$ is about 3.3-fold larger than that for the WT case. The obtained MM constant of the translation rate versus [EF-G] for $\Delta B8$ ($K_M^{(G)} = 800 \text{ nM}$) is about 11-fold larger than that for the WT case. By contrast, the experimental data show that the MM constant for the rate of the fast phase versus [EF-G] for $\Delta B8$ is about 25-fold larger than that for the WT case.

IV. DISCUSSION AND CONCLUSION

By comparing the theoretical results with the experimental data we have shown that the mutations ($\Delta B1a$, $\Delta B4$, $\Delta B7a$, and $\Delta B8$) reduce the affinity for EF-G-GTP via decreasing the binding rate of EF-G-GTP and increasing the release rate of EF-G-GTP (or EF-G-GDP-Pi), increase the transition rate k_3 from the classical nonrotated pretranslocation state to the hybrid state, and increase the transition rate k_4 from the hybrid state to the post-translocation state. The implications of the effect of the mutations on the transition rate k_3 were studied in Sec. III B. In the following we discuss the implications of the effect of the mutations on the transition rate k_4 and on the EF-G binding.

In our model (Fig. 1) the transition rate k_4 is approximately equal to the rate of the ribosomal unlocking and is also approximately equal to the rate of the fast phase for the forward mRNA translocation [see Eq. (10) under $k_{-3} \ll k_3 < k_4$]. Thus, the mutation-induced increase in the rate of the fast phase results from the increase in the rate of the ribosomal unlocking. Our theoretical data show that the transition rate k_4 for $\Delta B1a$, $\Delta B4$, $\Delta B7a$, and $\Delta B8$ is increased, respectively, by about 4.5-fold, 3.7-fold, 2.3-fold, and 3.3-fold relative to that for the WT ribosome. It is noted here that these degrees of increase in k_4 are inconsistent with those in k_3 and k_b , implying that the increase in k_4 could not be due to the reduction in the energy barrier ΔE . Previous structural studies implicated that the intrasubunit rotation, i.e., the forward rotation of the 30S head relative to the 30S body, induces the ribosomal unlocking [42–46]. Thus, our results indicate that one of the effects of the mutation on the ribosomal unlocking could be via the intrasubunit rotation.

The available structural studies [45,46] showed that EF-G binds to the interface between the 50S and 30S subunits. It is thus understandable that the mutations of the intersubunit bridge affect the binding of EF-G.

Based on the elongation pathway that is proposed based on our results on the kinetics of EF-G-dependent mRNA translocation, we calculated the translation rate versus concentrations of EF-G-GTP and the ternary complex for WT and mutant ribosomes $\Delta B1a$, $\Delta B4$, $\Delta B7a$, and $\Delta B8$. It was shown that the dependence of the translation rate on the concentration of EF-G-GTP does not follow the MM kinetics, whereas the dependence of the translation rate on the concentration of the ternary complex follows the MM kinetics. This property that the translation rate versus EF-G-GTP concentration for the ribosome does not follow the MM kinetics is in sharp contrast to the general property for other enzymes that the rate of the enzymatic reaction versus the concentration of a substrate follows the MM kinetics [13,14,16]. It was revealed that this non-MM kinetics for the ribosome results from the intrinsic character of the spontaneous intersubunit rotations before EF-G-GTP binding. In addition, we mentioned that the predicted results of the translation rate versus EF-G-GTP concentration [Figs. 6(a), 6(c), and 7] could be tested easily in future experiments. A straightforward comparison of the predicted results with the experimental data would have important implications for our understanding of the molecular mechanism of the ribosome elongation.

Finally, it is mentioned that the studies presented here not only deepen our understanding of the molecular mechanism of the ribosomal translocation, but also provide strategies for the design and fabrication of the relevant nanomachine. For example, it was shown that enhancing the rates of the intersubunit rotations, which is realized by the mutations to some intersubunit bridges such as B1a, B4, B7a, and B8 in the native ribosome, can increase the translation rate (comparing Fig. 6 with Fig. 7). This is also relevant to the general physical analysis with a stochastic microswimming model for the translational velocity of the ribosome, assuming simply that its two subunits are subject to stochastic rearrangements [47], where it was shown that the mean propulsion velocity of the ribosome depends sensitively on the transition rates among the different conformations.

ACKNOWLEDGMENT

This work was supported by the National Natural Science Foundation of China (Grant No. 11374352).

APPENDIX A: DERIVATION OF THE EQUATION OF THE MEAN TIME FOR TRANSITION FROM STATE 01 TO STATE 3 DURING THE ELONGATION CYCLE

At steady state, Eqs. (2)–(4) are written as

$$k_{01}P_{01} - (k_{-01} + k_2)P_{02} + k_{-2}P_2 = 0, \quad (\text{A1})$$

$$k_1P_{01} - (k_{-1} + k_3)P_1 + k_{-3}P_2 = 0, \quad (\text{A2})$$

$$k_2P_{02} + k_3P_1 - (k_{-2} + k_{-3} + k_4)P_2 = 0. \quad (\text{A3})$$

The mean time τ_2 for transition from state 01 to state 3 is calculated by

$$\tau_2 = \frac{P_{01} + P_{02} + P_1 + P_2}{k_4P_2}. \quad (\text{A4})$$

From Eqs. (A1)–(A4), we finally obtain Eqs. (16)–(18).

APPENDIX B: EFFECT OF THE VARIATION OF HYBRID-STATE PROBABILITY ON BIPHASIC KINETICS OF EF-G-DEPENDENT mRNA TRANSLOCATION

As Eqs. (10)–(14) show, the variation of the hybrid-state probability a affects the values of the fraction amplitudes A_1 and A_2 , but it has no effect on the values of $\lambda_1^{(\max)}$ and $\lambda_2^{(\max)}$. Here it is interesting to study the effect of the variation of a on values of the MM constants $K_1^{(1/2)}$ and $K_2^{(1/2)}$ defined in Eq. (24). In the main text we considered the case with the value of $a = 0.582$ for the WT ribosome (Fig. 3). Here we consider the case with another value of $a = 0.73$. From Eqs. (12)–(14) we have $A_1 = 0.676$ and $A_2 = 0.324$ for $a = 0.73$. The numerical solution of Eqs. (1)–(5) shows that at any [EF-G], the results of $1 - P_3(t)$ versus time can also be well fitted by using the two-exponential function $1 - P_3(t) = A_1e^{-\lambda_1 t} + A_2e^{-\lambda_2 t}$, with fixed $A_1 = 0.676$ and $A_2 = 0.324$ [Figs. 8(a)–8(c)]. The results of λ_1 and λ_2 versus [EF-G] are shown in Fig. 8(d), which can be fitted to Eq. (24), with $\lambda_1^{(\max)} = 15 \text{ s}^{-1}$, $\lambda_2^{(\max)} = 2.4 \text{ s}^{-1}$, $K_1^{(1/2)} = 0.68 \mu\text{M}$, and

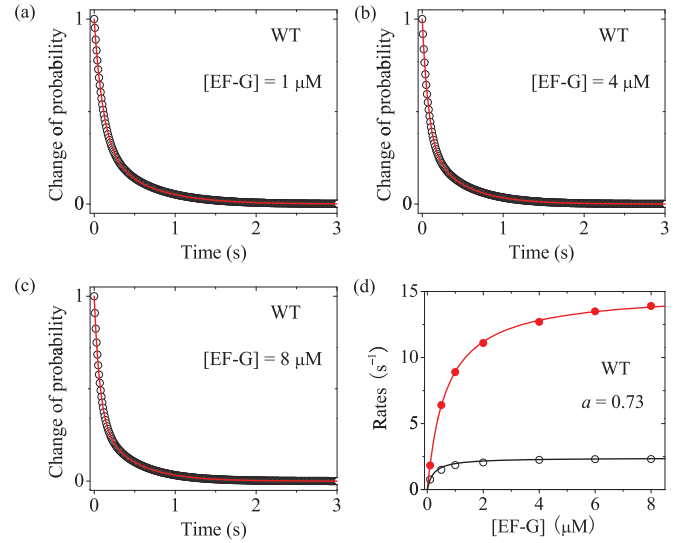


FIG. 8. (Color online) Results for the WT ribosome, with the probability of the hybrid state before EF-G-GTP binding being $a = 0.73$. (a)–(c) Change of the probability of post-translocation state $1 - P_3(t)$ versus time at different concentrations of EF-G-GTP. Dots represent calculated results and lines represent the fit curves with the two-exponential function $1 - P_3(t) = 0.676e^{-\lambda_1 t} + 0.324e^{-\lambda_2 t}$. (d) Rate of the fast phase λ_1 and rate of the slow phase λ_2 versus concentration of EF-G-GTP. Lines are fits to the MM equation $\lambda_{1,2} = \lambda_{1,2}^{(\max)} [\text{EF-G}] / ([\text{EF-G}] + K_{1,2}^{(1/2)})$, with $\lambda_1^{(\max)} = 15 \text{ s}^{-1}$, $\lambda_2^{(\max)} = 2.4 \text{ s}^{-1}$, $K_1^{(1/2)} = 0.68 \mu\text{M}$, and $K_2^{(1/2)} = 0.22 \mu\text{M}$.

$K_2^{(1/2)} = 0.22 \mu\text{M}$. These results and the results of Fig. 3 indicate that by increasing a from 0.582 to 0.73, the value of $K_1^{(1/2)}$ decreases only slightly from about $0.73 \mu\text{M}$ to about $0.68 \mu\text{M}$, while the value of $K_2^{(1/2)}$ is kept nearly unchanged. In Fig. 9 we show the results of the fraction amplitudes A_1 and A_2 and the MM constants $K_1^{(1/2)}$ and $K_2^{(1/2)}$ versus a . From these results we thus conclude that the MM constant for the rate of the fast phase versus [EF-G] only decreases slightly with the increase of a , while the MM constant for the rate of the slow phase versus [EF-G] is approximately independent of a .

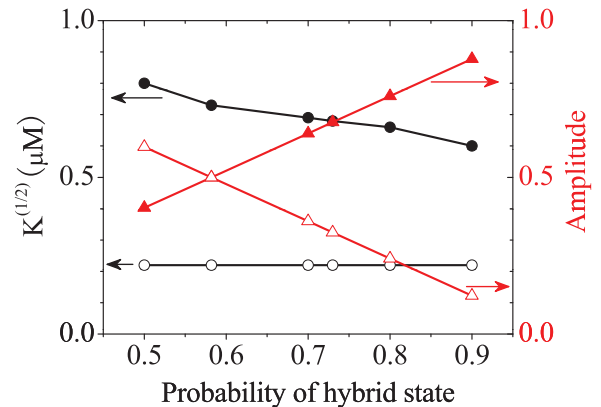


FIG. 9. (Color online) The MM constant $K^{(1/2)}$ for rates of the fast and slow phases of the forward mRNA translocation and the fraction amplitudes of the fast and slow phases versus the probability of the hybrid state before EF-G-GTP binding.

- [1] W. Wintermeyer, F. Peske, M. Beringer, K. B. Gromadski, A. Savelsbergh, and M. V. Rodnina, *Biochem. Soc. Trans.* **32**, 733 (2004).
- [2] K. B. Gromadski and M. V. Rodnina, *Mol. Cell* **13**, 191 (2004).
- [3] H. F. Noller, M. M. Yusupov, G. Z. Yusupova, A. Baucom, and J. H. D. Cate, *FEBS Lett.* **514**, 11 (2002).
- [4] J. Frank, H. Gao, J. Sengupta, N. Gao, and D. J. Taylor, *Proc. Natl. Acad. Sci. USA* **104**, 19671 (2007).
- [5] S. Shoji, S. E. Walker, and K. Fredrick, *ACS Chem. Biol.* **4**, 93 (2009).
- [6] M. V. Rodnina, A. Savelsbergh, V. I. Katunin, and W. Wintermeyer, *Nature (London)* **385**, 37 (1997).
- [7] P. Xie, *J. Theor. Biol.* **316**, 49 (2013).
- [8] Q. Liu and K. Fredrick, *Nucleic Acids Res.* **41**, 565 (2013).
- [9] F. Peske, A. Savelsbergh, V. I. Katunin, M. V. Rodnina, and W. Wintermeyer, *J. Mol. Biol.* **343**, 1183 (2004).
- [10] X. Shi, K. Chiu, S. Ghosh, and S. Joseph, *Biochemistry* **48**, 6772 (2009).
- [11] D. N. Ermolenko and H. F. Noller, *Nat. Struct. Mol. Biol.* **18**, 457 (2011).
- [12] A. Savelsbergh, V. I. Katunin, D. Mohr, F. Peske, M. V. Rodnina, and W. Wintermeyer, *Mol. Cell* **11**, 1517 (2003).
- [13] M. Dixon and E. C. Webb, *Enzymes* (Academic, New York, 1979).
- [14] D. Chowdhury, *Phys. Rep.* **529**, 1 (2013).
- [15] X. Qu, J.-D. Wen, L. Lancaster, H. F. Noller, C. Bustamante, and I. Tinoco, Jr., *Nature (London)* **475**, 118 (2011).
- [16] D. Chowdhury, *FEBS J.* **281**, 601 (2014).
- [17] P. Xie, *Biosystems* **118**, 1 (2014).
- [18] A. V. Zavialov and M. Ehrenberg, *Cell* **114**, 113 (2003).
- [19] D. Moazed and H. F. Noller, *Nature (London)* **342**, 142 (1989).
- [20] S. C. Blanchard, H. D. Kim, R. L. Gonzalez, Jr., J. D. Puglisi, and S. Chu, *Proc. Natl Acad. Sci. USA* **101**, 12893 (2004).
- [21] M. Valle, A. Zavialov, J. Sengupta, U. Rawat, M. Ehrenberg, and J. Frank, *Cell* **114**, 123 (2003).
- [22] J. Fei, P. Kosuri, D. D. MacDougall, and R. L. Gonzalez, Jr., *Mol. Cell* **30**, 348 (2008).
- [23] P. V. Cornish, D. N. Ermolenko, H. F. Noller, and T. Ha, *Mol. Cell* **30**, 578 (2008).
- [24] C. Chen, B. Stevens, J. Kaur, D. Cabral, H. Liu, Y. Wang, H. Zhang, G. Rosenblum, Z. Smilansky, Y. E. Goldman, and B. Cooperman, *Mol. Cell* **42**, 367 (2011).
- [25] P. Xie, *Biophys. Chem.* **180-181**, 22 (2013).
- [26] R. Lill, J. M. Robertson, and W. Wintermeyer, *EMBO J.* **8**, 3933 (1989).
- [27] J. S. Feinberg and S. Joseph, *Proc. Natl Acad. Sci. USA* **98**, 11120 (2001).
- [28] P. Xie, *Eur. Biophys. J.* **42**, 347 (2013).
- [29] P. Xie, *PLoS ONE* **8**, e70789 (2013).
- [30] J. Frank and R. K. Agrawal, *Nature (London)* **406**, 318 (2000).
- [31] I. Tinoco, Jr. and J. D. Wen, *Phys. Biol.* **6**, 025006 (2009).
- [32] A. K. Sharma and D. Chowdhury, *Phys. Biol.* **8**, 026005 (2011).
- [33] As mentioned above, this paper considers only the translation of the mRNA with homogeneous codons using *in vitro* assays containing only one species of the ternary complex and thus the competition of the cognate with near-cognate and noncognate ternary complexes is not considered. Consequently, the MM kinetics of the translation rate versus the concentration of the ternary complex presented here is only applicable to the case with no competition of the cognate with near-cognate and noncognate ternary complexes.
- [34] L. Wang, R. B. Altman, and S. C. Blanchard, *RNA* **17**, 2189 (2011).
- [35] As available SMFRET data [23] and theoretical analysis [29] have shown, the ribosome in the nonlabile state does not mean that the ribosome is in the fixed conformation. Rather, the ribosome can still transit between the nonrotated and rotated conformations, but with much lower transition rates than in the labile state.
- [36] S. E. Walker, S. Shoji, D. Pan, B. S. Cooperman, and K. Fredrick, *Proc. Natl. Acad. Sci. USA* **105**, 9192 (2008).
- [37] T. Pape, W. Wintermeyer, and M. V. Rodnina, *EMBO J.* **17**, 7490 (1998).
- [38] T. Pape, W. Wintermeyer, and M. V. Rodnina, *EMBO J.* **18**, 3800 (1999).
- [39] M. V. Rodnina, M. Beringer, and W. Wintermeyer, *Trends Biochem. Sci.* **32**, 20 (2007).
- [40] H. Stark, M. V. Rodnina, H. J. Wieden, F. Zemlin, W. Wintermeyer, and M. van Heel, *Nat. Struct. Biol.* **9**, 849 (2002).
- [41] B. Wilden, A. Savelsbergh, M. V. Rodnina, and W. Wintermeyer, *Proc. Natl Acad. Sci. USA* **103**, 13670 (2006).
- [42] B. S. Schuwirth, M. A. Borovinskaya, C. W. Hau, W. Zhang, A. Vila-Sanjurjo, J. M. Holton, and J. H. D. Cate, *Science* **310**, 827 (2005).
- [43] M. Selmer, C. M. Dunham, F. V. Murphy IV, A. Weixlbaumer, S. Petry, A. C. Kelley, J. R. Weir, and V. Ramakrishnan, *Science* **313**, 1935 (2006).
- [44] A. H. Ratje, J. Loerke, A. Mikolajka, M. Brunner, P. W. Hildebrand, A. L. Starosta *et al.*, *Nature (London)* **468**, 713 (2010).
- [45] D. S. Tourigny, I. S. Fernández, A. C. Kelley, and V. Ramakrishnan, *Science* **340**, 1235490 (2013).
- [46] J. Zhou, L. Lancaster, J. P. Donohue, and H. F. Noller, *Science* **340**, 1236086 (2013).
- [47] J. S. Gonzalez-Garcia and J. Delgado, *Phys. Rev. E* **88**, 012723 (2013).